Research Square

Preprints are preliminary reports that have not undergone peer review.
They should not be considered conclusive, used to inform clinical practice,
or referenced by the media as validated information.

A geometrically exact beam element via the gradient-deficient absolute nodal coordinate formulation

Baixun Shao
Yanshan University
Minggang Wu
Yanshan University
Yufeng Wang
Yanshan University
Zhenxing Shen
shenzx@ysu.edu.cn
Yanshan University

Research Article

Keywords: Absolute nodal coordinate formulation, gradient-deficient beam element, geometrically exact beam, degree of freedom reduction

Posted Date: April 24th, 2026

DOI: https://doi.org/10.21203/rs.3.rs-9279936/v1

License: This work is licensed under a Creative Commons Attribution 4.0 International License.
Read Full License

Additional Declarations: No competing interests reported.

A geometrically exact beam element via the gradient-deficient absolute nodal coordinate formulation

Baixun Shao, Minggang Wu, Yufeng Wang, Zhenxing Shen*

*Key Laboratory of Mechanical Reliability for Heavy Equipment and Large Structures of Hebei Province, School of Civil Engineering and Mechanics, Yanshan University, Qinhuangdao, 066004, China.

*Corresponding author(s). E-mail(s): shenzx@ysu.edu.cn;
Contributing authors: shaobx@stumail.ysu.edu.cn;
ruopeng@stumail.ysu.edu.cn; wangyf@stumail.ysu.edu.cn;

Abstract

Dynamic modeling of beam-like structures undergoing large rotations and deformations within the absolute nodal coordinate formulation (ANCF) often requires a large number of gradient-related degrees of freedom, leading to high computational cost. In this paper, a gradient-deficient geometrically exact ANCF beam element is proposed to achieve a more compact kinematic description while retaining the capability to represent essential deformation modes. The proposed formulation interpolates the axial gradient together with a single transverse gradient to construct a local Cartesian coordinate system for cross-sectional representation, thereby eliminating one redundant transverse gradient. Based on this kinematic framework, the elastic force vector and the generalized external force vectors corresponding to applied moments, concentrated forces, and distributed loads are formulated. Several numerical examples involving large-deflection bending, rolling-up deformation, and pure torsional loading are presented. The results indicate that the proposed element provides accuracy comparable to that of existing fully parameterized ANCF beam elements, while reducing the number of degrees of freedom and the overall computational scale.

Keywords: Absolute nodal coordinate formulation, gradient-deficient beam element, geometrically exact beam, degree of freedom reduction

1 Introduction

The accurate modeling of beam-like flexible structures undergoing large rotations and large deformations is a fundamental problem in computational mechanics and flexible multibody dynamics. In such problems, the kinematic description of beam deformation plays a central role in determining numerical accuracy, and computational efficiency. Classical geometrically exact beam theories provide a clear and physically consistent description of large displacements and rotations while maintaining a relatively compact set of kinematic variables. Owing to these advantages, geometrically exact beam formulations have been widely applied in the analysis of flexible structures experiencing strong geometric nonlinearities, such as aerospace structures, robotic manipulators, and slender mechanical components undergoing large overall motions [1–4].

Over the past decades, geometrically exact beam formulations have been further developed and refined, establishing a reliable framework for the large-deformation analysis of slender structures [5–7]. However, to describe the orientation of beam cross sections, most geometrically exact beam formulations rely on finite rotation parameterizations, with common choices including Euler angles, Cardan angles, Euler parameters, and quaternions [8–10]. These parameterizations are not additive in nature and therefore do not form a closed vector space, which may lead to singular configurations, parameter coupling, and numerical complications in simulations involving large accumulated rotations or long-term dynamic integration [10–12].

To overcome the difficulties associated with rotational parameters, the absolute nodal coordinate formulation (ANCF) was introduced as an alternative geometrically exact approach for flexible multibody systems [13]. In ANCF, global nodal positions and their gradient vectors are adopted as generalized coordinates, thereby completely eliminating rotational variables and avoiding the singularity issues inherent in rotation-based formulations [14–16]. Building upon these advantages, numerous ANCF beam formulations have been developed for modeling slender structures undergoing large rotations and deformations. These developments include spatial ANCF beam elements capable of representing coupled axial-bending-torsional behaviors [17, 18], refined curvature descriptions and higher-order interpolation schemes for improved bending accuracy and numerical efficiency [19–21], as well as enhanced formulations to capture cross-sectional effects and alleviate numerical locking phenomena [22–28]. Comparative studies indicate that the adopted curvature representation and cross-sectional kinematics strongly influence the accuracy of large-displacement ANCF beam analysis [29]. Despite these advances, the improved accuracy of conventional ANCF beam elements is generally achieved at the expense of a large number of gradient-related degrees of freedom. The inclusion of multiple gradient vectors at each node leads to high-dimensional nonlinear governing equations, resulting in substantial computational cost and limited efficiency in large-scale applications [30].

Recognizing that the excessive computational cost of ANCF beam elements primarily originates from redundant gradient-related degrees of freedom, considerable research efforts have been devoted to the development of gradient-deficient formulations [31–35]. Early studies systematically analyzed deformation modes in ANCF beam elements and demonstrated that a consistent reduction of gradient degrees of freedom can significantly improve numerical efficiency without violating geometric exactness or

energy consistency [36, 37]. Subsequently, a variety of gradient-deficient ANCF beam elements and reduced cross-sectional coordinate descriptions have been proposed to alleviate numerical complexity while retaining essential deformation mechanisms, particularly bending and torsional behaviors [38–42]. However, many of the previously proposed gradient-deficient formulations are unable to accurately represent torsional deformation, or their capability in describing torsion remains limited, and some are further tailored to specific cross-sectional geometries or rely on additional kinematic assumptions, which may restrict their general applicability [43]. Overall, these studies suggest that a judicious reduction of gradient vectors holds significant promise for developing a more compact and computationally efficient geometrically exact beam formulation within the ANCF framework.

Despite these advances, constructing a gradient-deficient ANCF beam formulation that simultaneously retains accurate torsional deformation capability, avoids rotational parameters, and maintains a clear and physically interpretable kinematic description remains a challenging task. In particular, the efficient construction of a local cross-sectional coordinate system using a minimal set of gradient vectors is crucial for further reducing computational complexity without compromising essential deformation characteristics.

To address this issue, this paper proposes a gradient-deficient geometrically exact beam element within the framework of the ANCF. The proposed element interpolates the axial gradient together with a single transverse gradient to construct a local Cartesian coordinate system for cross-sectional description. By eliminating one redundant transverse gradient, the formulation achieves a reduced number of degrees of freedom while preserving the ability to accurately represent cross-sectional geometry and torsional deformation. The proposed approach aims to provide a compact and efficient ANCF beam element suitable for large-rotation and large-deformation analyses.

The remainder of this paper is organized as follows: Section 2 presents the kinematic description and derivation of the proposed beam element. Section 3 presents the formulation of the elastic force vector. Section 4 presents the formulation of the generalized external forces due to external loads and moments. Section 5 provides numerical examples and discussions, and Section 6 concludes this paper.

2 Kinematics of the gradient-deficient ANCF beam element

The kinematic description of the cross-sectional coordinate system in geometrically exact beam theories has reached a relatively mature stage, with well-established formulations such as three-dimensional frame representations and independent interpolations of the beam centerline and cross-section [36, 40].

The global position vector $\mathbf{r}$ of an arbitrary point on the gradient-deficient beam, as illustrated in Fig. 1, is expressed as

$$\mathbf{r}(x, y, z) = \mathbf{r}_0(x) + y\,\mathbf{n}(x) + z\,\mathbf{b}(x) \tag{1}$$

where $\mathbf{r}_0$ represents the global position vector of the centroidal axis of the cross section. and $\mathbf{n}$ and $\mathbf{b}$ are orthonormal vectors defined in the cross-section with respect to the beam axis. Together with the unit tangent vector $\mathbf{t}$, they form the cross-sectional coordinate system, which can be written as

$$\mathbf{t} = \frac{\mathbf{r}_0'}{\|\mathbf{r}_0'\|}, \quad \mathbf{n} = \frac{\mathbf{r}_z \times \mathbf{t}}{\|\mathbf{r}_z \times \mathbf{t}\|}, \quad \mathbf{b} = \mathbf{t} \times \mathbf{n} \tag{2}$$

where the superscript $(\cdot)'$ denotes the derivative of a vector with respect to x, and the vector $\mathbf{r}_z$ represents the independent partial derivative of $\mathbf{r}$ with respect to z.

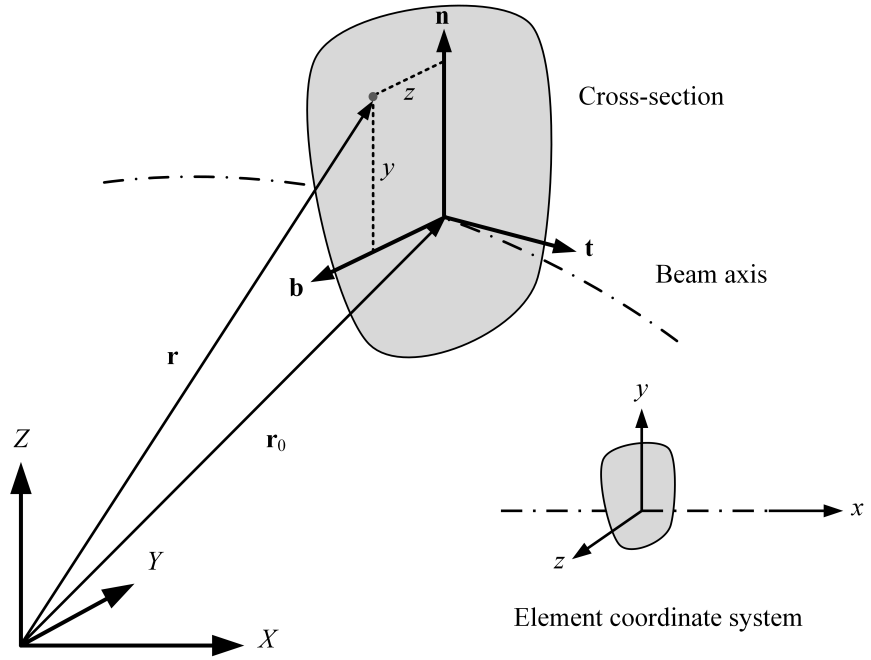


Fig. 1 Kinematic description of the gradient-deficient beam element.

Accordingly, the following nodal coordinate vector can be adopted

$$\mathbf{q}^k = \left[(\mathbf{r}^k)^{\mathrm{T}} \ (\mathbf{r}_x^k)^{\mathrm{T}} \ (\mathbf{r}_z^k)^{\mathrm{T}}\right]^{\mathrm{T}} \tag{3}$$

where, $\mathbf{r}^k$ represents the global position vector of node k, and $\mathbf{r}_x^k$ and $\mathbf{r}_z^k$ denote the gradients of the position vector at node k. The finite element discretizations of the centerline position vector and the cross-sectional direction vector employed in this work are defined as

$$\begin{aligned} \mathbf{r}_0 &= \mathbf{S}_0\mathbf{q}, \\ \mathbf{r}_z &= \mathbf{S}_z\mathbf{q} \end{aligned} \tag{4}$$

where the corresponding shape functions are given by Hermite interpolation and linear interpolation, respectively, and can be expressed as

$$\begin{aligned}\mathbf{S}_0 &= \left[\left(1-3\xi^2+2\xi^3\right)\mathbf{I}\ l\left(\xi-2\xi^2+\xi^3\right)\mathbf{I}\ \mathbf{0}\ \left(3\xi^2-2\xi^3\right)\mathbf{I}\ l\left(-\xi^2+\xi^3\right)\mathbf{I}\ \mathbf{0}\right], \\ \mathbf{S}_z &= \left[\mathbf{0}\ \mathbf{0}\ (1-\xi)\,\mathbf{I}\ \mathbf{0}\ \mathbf{0}\ \xi\mathbf{I}\right]\end{aligned} \tag{5}$$

in which $\xi = x/l$, l is the element length, and $\mathbf{I}$ and $\mathbf{0}$ are the 3×3 identity and zero matrices, respectively.

3 Elastic forces

The Biot strain tensor $\mathbf{E}_B$ is adopted in this work as the primary strain measure for subsequent derivations. It is a second-order tensor, whose components in the Cartesian coordinate system are denoted by $\mathbf{E}_{Bij}$, where $i,j = 1,2,3$. Considering the polar decomposition of the deformation gradient $\mathbf{F}$, it can be written as

$$\mathbf{F} = \mathbf{R}\mathbf{U} \tag{6}$$

where $\mathbf{R}$ is the orthogonal tensor associated with the cross-sectional coordinate system defined in the preceding section, and $\mathbf{U}$ is the right stretch tensor can be expressed as

$$\mathbf{U} = \mathbf{R}^{\mathrm{T}}\mathbf{F} = \begin{bmatrix} \mathbf{t}^{\mathrm{T}}(\mathbf{r}_0' + y\mathbf{n}' + z\mathbf{b}') & 0 & 0 \\ z\,\mathbf{n}^{\mathrm{T}}\mathbf{b}' & 1 & 0 \\ y\,\mathbf{b}^{\mathrm{T}}\mathbf{n}' & 0 & 1 \end{bmatrix}. \tag{7}$$

Substituting into the definition of the Biot strain tensor yields the following expression in terms of the deformation gradient and the rotation tensor as

$$E_{B\,ij} = U_{ij} - \delta_{ij} \tag{8}$$

where δ_{ij} is the Kronecker delta. The normal and shear strain components can be directly identified as

$$\begin{aligned}\varepsilon_{xx} &= \mathbf{t}^{\mathrm{T}}\mathbf{r}_0' - 1 + y\mathbf{t}^{\mathrm{T}}\mathbf{n}' + z\mathbf{t}^{\mathrm{T}}\mathbf{b}', \\ \gamma_{xy} &= -z\mathbf{b}^{\mathrm{T}}\mathbf{n}', \\ \gamma_{xz} &= y\mathbf{b}^{\mathrm{T}}\mathbf{n}'\end{aligned} \tag{9}$$

these strain components can be further expressed in terms of the axial strain and curvature measures as

$$\begin{aligned}\varepsilon_{xx} &= \varepsilon_0 + y\kappa_z - z\kappa_y, \\ \gamma_{xy} &= -z\kappa_x, \\ \gamma_{xz} &= y\kappa_x\end{aligned} \tag{10}$$

where ε_0, κ_x, κ_y, and κ_z denote the axial strain and curvature measures, respectively. These quantities are defined as [37]

$$\begin{aligned}
\varepsilon_0 &= \|\mathbf{r}_0'\| - 1, \\
\kappa_x &= \mathbf{b} \cdot \mathbf{n}' = \frac{(\mathbf{t} \cdot \mathbf{r}_z)(\mathbf{n} \cdot \mathbf{t}') - \mathbf{n} \cdot \mathbf{r}_z'}{\|\mathbf{c}\|}, \\
\kappa_y &= \mathbf{b} \cdot \mathbf{t}' = \frac{\mathbf{r}_z \cdot \mathbf{t}'}{\|\mathbf{c}\|}, \\
\kappa_z &= \mathbf{t} \cdot \mathbf{n}' = \frac{\mathbf{t} \cdot (\mathbf{r}_z \times \mathbf{t}')}{\|\mathbf{c}\|}
\end{aligned} \tag{11}$$

where

$$\mathbf{c} = \mathbf{r}_z \times \mathbf{t}. \tag{12}$$

Substituting the above strain measures into the strain energy expression and integrating over the cross-section, the total strain energy can be written in a compact form as

$$U = \frac{1}{2} \int_0^l \boldsymbol{\varepsilon}^{\mathrm{T}} \mathbf{D} \boldsymbol{\varepsilon} \, \mathrm{d}x \tag{13}$$

where the generalized strain vector and the constitutive matrix are given by

$$\begin{aligned}
\boldsymbol{\varepsilon} &= \begin{bmatrix} \varepsilon_0 & \kappa_y & \kappa_z & \kappa_x \end{bmatrix}^{\mathrm{T}}, \\
\mathbf{D} &= \mathrm{diag}\begin{pmatrix} EA & EI_y & EI_z & GI_{\mathrm{p}} \end{pmatrix}
\end{aligned} \tag{14}$$

with I_y and I_z being the second moments of area about the principal axes of the cross-section, and I_p the polar moment of inertia. The resulting formulation naturally leads to a decoupled representation of axial, bending, and torsional energies.

Taking the variation of the strain energy with respect to the generalized coordinates $\mathbf{q}$, the elastic force vector $\mathbf{Q}$ can be written in a compact form as

$$\mathbf{Q} = \frac{\partial U}{\partial \mathbf{q}} = \int_0^l \mathbf{B}^{\mathrm{T}} \mathbf{D} \boldsymbol{\varepsilon} \, \mathrm{d}x \tag{15}$$

in which the matrix $\mathbf{B}$ follows directly from the differentiation of the strain measures with respect to $\mathbf{q}$

$$\mathbf{B} = \frac{\partial \boldsymbol{\varepsilon}}{\partial \mathbf{q}} = \begin{bmatrix} \frac{\partial \varepsilon_0}{\partial \mathbf{q}} & \frac{\partial \kappa_y}{\partial \mathbf{q}} & \frac{\partial \kappa_z}{\partial \mathbf{q}} & \frac{\partial \kappa_x}{\partial \mathbf{q}} \end{bmatrix}^{\mathrm{T}} \tag{16}$$

where the corresponding components are given by

$$\frac{\partial \varepsilon_0}{\partial \mathbf{q}} = \frac{1}{\|\mathbf{r}_0'\|} \mathbf{S}_0'^{\mathrm{T}} \mathbf{r}_0' \tag{17}$$

$$\frac{\partial \kappa_y}{\partial \mathbf{q}} = \frac{1}{\|\mathbf{c}\|} \left(\mathbf{S}_z^{\mathrm{T}} \mathbf{t}' + \frac{\partial \mathbf{t}'^{\mathrm{T}}}{\partial \mathbf{q}} \mathbf{r}_z \right) - \frac{1}{\|\mathbf{c}\|^2} (\mathbf{r}_z \cdot \mathbf{t}') \frac{\partial \mathbf{c}^{\mathrm{T}}}{\partial \mathbf{q}} \mathbf{n} \tag{18}$$

$$\frac{\partial \kappa_z}{\partial \mathbf{q}} = \frac{1}{\|\mathbf{c}\|}\left[\frac{\partial \mathbf{t}^{\mathrm{T}}}{\partial \mathbf{q}}(\mathbf{r}_z \times \mathbf{t}') + \frac{\partial (\mathbf{r}_z \times \mathbf{t}')^{\mathrm{T}}}{\partial \mathbf{q}}\mathbf{t}\right] - \frac{1}{\|\mathbf{c}\|^3}\mathbf{t}\cdot(\mathbf{r}_z \times \mathbf{t}')\frac{\partial \mathbf{c}^{\mathrm{T}}}{\partial \mathbf{q}}\mathbf{c} \tag{19}$$

$$\begin{aligned}\frac{\partial \kappa_x}{\partial \mathbf{q}} = \frac{1}{\|\mathbf{c}\|}\Bigg[&\left(\mathbf{t}^{\mathrm{T}}\mathbf{r}_z\right)\left(\frac{\partial \mathbf{n}^{\mathrm{T}}}{\partial \mathbf{q}}\mathbf{t}' + \frac{\partial \mathbf{t}'^{\mathrm{T}}}{\partial \mathbf{q}}\mathbf{n}\right) + \left(\mathbf{n}^{\mathrm{T}}\mathbf{t}'\right)\left(\frac{\partial \mathbf{t}^{\mathrm{T}}}{\partial \mathbf{q}}\mathbf{r}_z + \mathbf{S}_z^{\mathrm{T}}\mathbf{t}\right)\\ &- \left(\frac{\partial \mathbf{n}^{\mathrm{T}}}{\partial \mathbf{q}}\mathbf{r}_z' + \mathbf{S}_z'^{\mathrm{T}}\mathbf{n}\right)\Bigg] - \frac{1}{\|\mathbf{c}\|^3}\left[(\mathbf{t}\cdot\mathbf{r}_z)(\mathbf{n}\cdot\mathbf{t}') - \mathbf{n}\cdot\mathbf{r}_z'\right]\frac{\partial \mathbf{c}^{\mathrm{T}}}{\partial \mathbf{q}}\mathbf{c}.\end{aligned} \tag{20}$$

4 Generalized external forces

The generalized external forces are derived within the framework of the principle of virtual work. Starting from the virtual work of external actions, the associated contributions are expressed in terms of the virtual kinematic quantities, which are consistently represented using the cross-sectional basis vectors. These quantities are then related to the nodal degrees of freedom through the interpolation of the global position vector. The detailed derivation of the corresponding generalized forces is presented in the following.

Consider a concentrated force $\mathbf{F}_P$ acting at a material point P within the element. The associated virtual work can be expressed as

$$\delta W_P = \mathbf{F}_P^{\mathrm{T}}\delta \mathbf{r}_P = \mathbf{F}_P^{\mathrm{T}}\left(\mathbf{S}_0(x_p) + y_p\frac{\partial \mathbf{n}}{\partial \mathbf{q}^{\mathrm{T}}} + z_p\frac{\partial \mathbf{b}}{\partial \mathbf{q}^{\mathrm{T}}}\right)\delta \mathbf{q} \tag{21}$$

where the derivatives of the basis vectors with respect to the position coordinates can be further written explicitly as

$$\frac{\partial \mathbf{n}^{\mathrm{T}}}{\partial \mathbf{q}} = \frac{1}{\|\mathbf{c}\|}\frac{\partial \mathbf{c}^{\mathrm{T}}}{\partial \mathbf{q}} - \frac{1}{\|\mathbf{c}\|^3}\frac{\partial \mathbf{c}^{\mathrm{T}}}{\partial \mathbf{q}}\mathbf{c}\mathbf{c}^{\mathrm{T}} \tag{22}$$

$$\begin{aligned}\frac{\partial \mathbf{b}^{\mathrm{T}}}{\partial \mathbf{q}} = \frac{1}{\|\mathbf{c}\|}&\left[\mathbf{S}_z^{\mathrm{T}} - \left(\mathbf{t}^{\mathrm{T}}\mathbf{r}_z\right)\frac{\partial \mathbf{t}^{\mathrm{T}}}{\partial \mathbf{q}} - \left(\frac{\partial \mathbf{t}^{\mathrm{T}}}{\partial \mathbf{q}}\mathbf{r}_z + \mathbf{S}_z^{\mathrm{T}}\mathbf{t}\right)\mathbf{t}^{\mathrm{T}}\right]\\ &- \frac{1}{\|\mathbf{c}\|^3}\frac{\partial \mathbf{c}^{\mathrm{T}}}{\partial \mathbf{q}}\mathbf{c}\Big[\mathbf{r}_z - (\mathbf{t}^{\mathrm{T}}\mathbf{r}_z)\mathbf{t}\Big]^{\mathrm{T}}\end{aligned} \tag{23}$$

where

$$\frac{\partial \mathbf{t}^{\mathrm{T}}}{\partial \mathbf{q}} = \frac{1}{\|\mathbf{r}_0'\|}\mathbf{S}_0'^{\mathrm{T}} - \frac{1}{\|\mathbf{r}_0'\|^3}\mathbf{S}_0'^{\mathrm{T}}\mathbf{r}_0'\mathbf{r}_0'^{\mathrm{T}} \tag{24}$$

and the generalized force corresponding to the concentrated force can be expressed as

$$\mathbf{Q}_P = \left(\mathbf{S}_0(x_p) + y_p\frac{\partial \mathbf{n}}{\partial \mathbf{q}^{\mathrm{T}}} + z_p\frac{\partial \mathbf{b}}{\partial \mathbf{q}^{\mathrm{T}}}\right)^{\mathrm{T}}\mathbf{F}_P. \tag{25}$$

By extending this formulation to a distributed force $\mathbf{F}_V(x, y, z)$ acting throughout the beam, the generalized external force vector can be obtained by integrating its

contributions over the entire volume V, yielding

$$\mathbf{Q}_V = \int_V \left(\mathbf{S}_0(x) + y\frac{\partial \mathbf{n}}{\partial \mathbf{q}^{\mathrm{T}}} + z\frac{\partial \mathbf{b}}{\partial \mathbf{q}^{\mathrm{T}}} \right)^{\mathrm{T}} \mathbf{F}_V \, \mathrm{d}x \, \mathrm{d}y \, \mathrm{d}z. \tag{26}$$

Consider the virtual rotational displacement $\delta\gamma_y$ associated with the torsional deformation of the beam cross-section induced by the bending moment M_y, as illustrated in Fig. 2. This virtual rotational displacement can be expressed in terms of the virtual nodal coordinate vector through the intermediate representation of the virtual coordinate gradients as

$$\delta\gamma_y = \left(\frac{b_3}{b_1^2 + b_3^2}\frac{\partial b_1}{\partial \mathbf{q}^{\mathrm{T}}} - \frac{b_1}{b_1^2 + b_3^2}\frac{\partial b_3}{\partial \mathbf{q}^{\mathrm{T}}} \right) \delta\mathbf{q}. \tag{27}$$

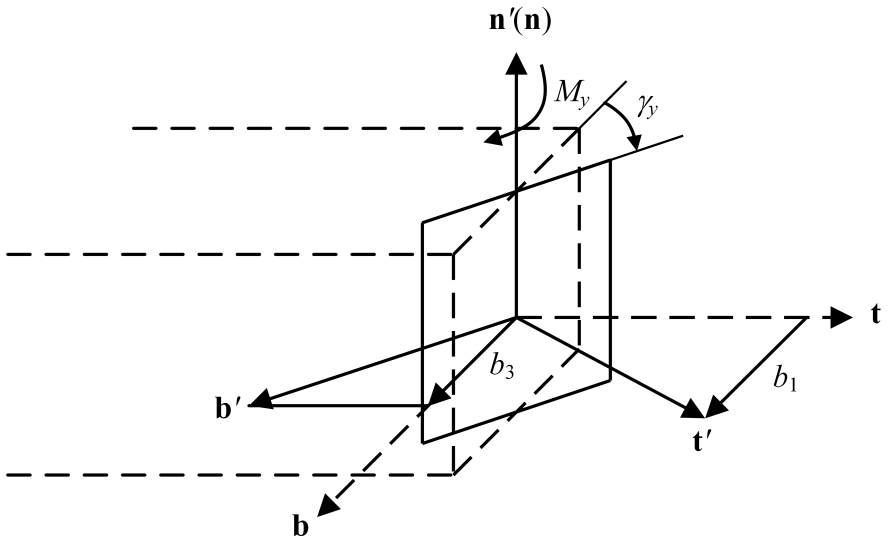


Fig. 2 Bending diagram and cross-sectional deflection of a gradient-deficient beam element under bending moment.

The virtual work associated with the applied moment vector $\mathbf{M} = [M_x, M_y, M_z]^{\mathrm{T}}$ can be expressed in compact form as

$$\delta W_M = \mathbf{M}^{\mathrm{T}}\delta\boldsymbol{\gamma} = \mathbf{M}^{\mathrm{T}}\mathbf{G}(\mathbf{q})\delta\mathbf{q} \tag{28}$$

where $\boldsymbol{\gamma} = [\gamma_x \ \gamma_y \ \gamma_z]^{\mathrm{T}}$ denotes the generalized rotational variation vector, $\mathbf{G}(\mathbf{q})$ is the corresponding kinematic transformation matrix can be written as

$$\mathbf{G}(\mathbf{q}) = \begin{bmatrix} \left(\frac{n_2}{n_2^2+n_3^2} \frac{\partial n_3}{\partial \mathbf{q}^{\mathrm{T}}} - \frac{n_3}{n_2^2+n_3^2} \frac{\partial n_2}{\partial \mathbf{q}^{\mathrm{T}}} \right) \\ \left(\frac{b_3}{b_1^2+b_3^2} \frac{\partial b_1}{\partial \mathbf{q}^{\mathrm{T}}} - \frac{b_1}{b_1^2+b_3^2} \frac{\partial b_3}{\partial \mathbf{q}^{\mathrm{T}}} \right) \\ \left(-\frac{n_2}{n_1^2+n_2^2} \frac{\partial n_1}{\partial \mathbf{q}^{\mathrm{T}}} + \frac{n_1}{n_1^2+n_2^2} \frac{\partial n_2}{\partial \mathbf{q}^{\mathrm{T}}} \right) \end{bmatrix} \tag{29}$$

the generalized force corresponding to the applied moment can be expressed as

$$\mathbf{Q}_M = \mathbf{G}(\mathbf{q})^{\mathrm{T}} \mathbf{M}. \tag{30}$$

5 Numerical examples

This section presents several benchmark problems to examine the performance of the proposed gradient-deficient beam element under large deformation and torsional loading. The results are compared with analytical solutions or well-established reference results from the literature.

5.1 Convergence verification

A static bending problem of a cantilever beam subjected to its own weight G is first considered to examine the convergence behavior of the proposed element. The beam has a length of $L = 1$ m, a square cross-section of 0.01 m$\times$0.01 m, a Young's modulus of $E = 2.077 \times 10^{11}$ Pa, and a material density of $\rho = 7800$ kg/m^3. According to classical strength-of-materials theory, the vertical deflection at the free end of a cantilever beam under self-weight can be expressed analytically as

$$f = \frac{mgL^3}{8EI}. \tag{31}$$

Discretize the beam into 1, 2, 4, 6, and 8 elements, respectively. Fig. 3 compares the numerically obtained free-end deflections with the analytical solution. The results show that the proposed beam element converges rapidly as the mesh is refined. With eight elements, the numerical solution closely approaches the analytical value, has an error of only 0.00248%, indicating satisfactory convergence characteristics.

5.2 Free-end loading of a cantilever beam

To further examine the static large-deformation response, a cantilever beam subjected to a concentrated force at the free end is analyzed, as illustrated in Fig. 4. The beam geometry and material properties are identical to those used in the convergence study [29], it has a length of $L = 10$ m, a square cross-section of 0.1 m $\times$ 0.1 m, a Young's modulus of $E = 2.1 \times 10^{11}$ Pa, and the beam is discretized into ten elements.

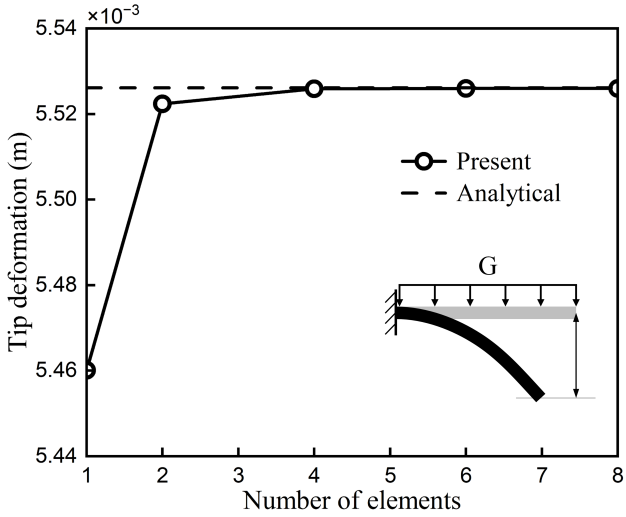


Fig. 3 Deformation of the free end under different numbers of elements.

The force applied at the free end is given by

$$F = \lambda \frac{EI_y}{L^2} \tag{32}$$

where $\lambda = 1.0, 2.0, \ldots, 10.0$ is a dimensionless parameter for the applied concentrated load.

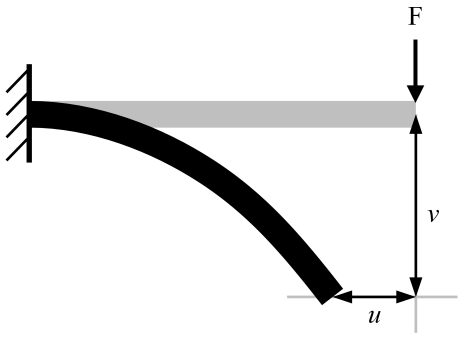


Fig. 4 Cantilever beam subjected to a concentrated force at the free end.

The numerical results are compared with the reference solutions reported by Zhang and Luo [29], which were obtained using exact and general curvature formulations and validated against the reference model results of Mattiasson [44]. The exact curvature formulation evaluates the curvature by differentiating the unit tangent vector with respect to the arc length, whereas the general curvature formulation is constructed

based on the orthogonality between the tangent and curvature vectors. Tables 1 and 2 summarize the axial and transverse displacements at the free end for different load levels.

Table 1 Axial displacement at the free end (u/L) for different models

λ	Reference [44]	Exact curvature [29]	General curvature [29]	Present
1.0	0.05643	0.05643	0.05643	0.05643
2.0	0.16064	0.16060	0.16060	0.16060
3.0	0.25442	0.25433	0.25434	0.25434
4.0	0.32894	0.32880	0.32881	0.32880
5.0	0.38763	0.38744	0.38744	0.38744
6.0	0.43459	0.43435	0.43435	0.43435
7.0	0.47293	0.47263	0.47264	0.47263
8.0	0.50483	0.50448	0.50449	0.50448
9.0	0.53182	0.53143	0.53144	0.53143
10.0	0.55500	0.55455	0.55456	0.55455

Table 2 Transverse displacement at the free end (v/L) for different models

λ	Reference [44]	Exact curvature [29]	General curvature [29]	Present
1.0	0.30172	0.30171	0.30171	0.30171
2.0	0.49346	0.49339	0.49339	0.49339
3.0	0.60325	0.60313	0.60313	0.60312
4.0	0.66996	0.66977	0.66977	0.66977
5.0	0.71379	0.71353	0.71354	0.71353
6.0	0.74457	0.74425	0.74425	0.74424
7.0	0.76737	0.76698	0.76698	0.76698
8.0	0.78498	0.78453	0.78453	0.78453
9.0	0.79906	0.79854	0.79854	0.79854
10.0	0.81061	0.81003	0.81003	0.81003

Fig. 5 present the relative error between various models and the reference solution, defined as

$$\psi = \left| \frac{\mu - \mu_{\text{ref}}}{\mu_{\text{ref}}} \right| \tag{33}$$

where μ and μ_{ref} denote the results obtained from the considered model and the reference solution, respectively, and ψ represents the relative error. Close agreement between the present results and the reference solutions is observed over the entire loading range. This indicates that the present model is capable of accurately reproducing the benchmark solutions and maintains a level of accuracy comparable to both the exact and general curvature formulations. In particular, the differences among the three models remain negligible, demonstrating that the proposed formulation preserves the essential deformation characteristics required for the analysis of beams undergoing moderate geometric nonlinearity.

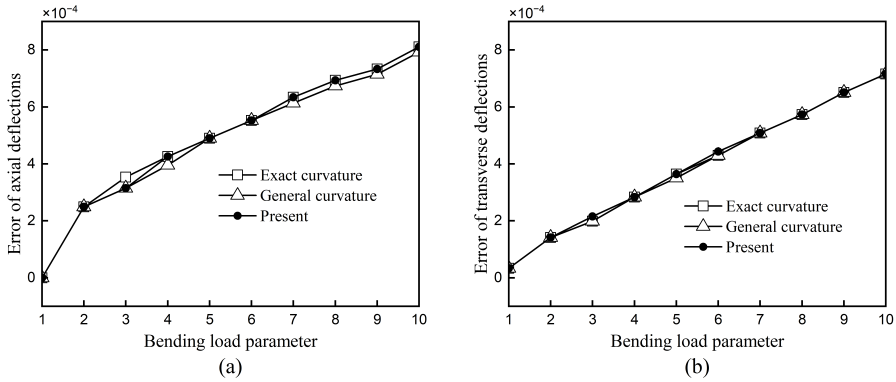


Fig. 5 Comparison of relative errors deflections predicted by the exact curvature model, general curvature model, and the present model under different non-dimensional bending load parameters: (a) relative error of axial displacement, (b) relative error of transverse displacement.

5.3 Rolling-up problem of a cantilever beam

A highly nonlinear bending problem is next considered, in which a horizontal cantilever beam is progressively bent into a circular configuration under a pure bending moment applied at the free end, as shown in Fig. 6. This problem is commonly used to assess the ability of beam elements to capture large rotations and curvature effects. The beam parameters are identical to those in the free-end loading case, and the beam is discretized into nine elements. The force applied at the free end is given by

$$M = \lambda \frac{\pi E I_y}{L} \tag{34}$$

where $\lambda = 0.2, 0.4, \ldots, 2.0$ is a dimensionless parameter, with $\lambda = 2.0$ corresponding to a fully circular configuration of the beam.

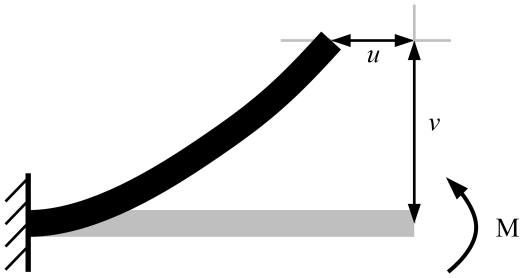


Fig. 6 Cantilever beam subjected to a pure bending moment at the free end.

The numerical results are compared with the reference model results reported by Sonneville and Bruels [45] and the ANCF results presented by Zhang and Luo [29]. The axial and transverse displacements of the free end are listed in Tables 3 and 4.

Fig. 7 illustrates the relative error with respect to the analytical solution. As the bending moment increases, the deviation from the analytical solution gradually grows,

Table 3 Axial displacement at the free end (u/L) for different models

λ	Reference [44]	Exact curvature [29]	General curvature [29]	Present
0.2	0.064511	0.064509	0.056249	0.064511
0.4	0.243173	0.243170	0.212316	0.243172
0.6	0.495449	0.495445	0.434926	0.495441
0.8	0.766128	0.766118	0.680982	0.766096
1.0	1.000000	0.999997	0.908379	0.999935
1.2	1.155915	1.155872	1.084062	1.155830
1.4	1.216236	1.216240	1.188994	1.216223
1.6	1.189207	1.189401	1.219971	1.189441
1.8	1.103943	1.104497	1.188226	1.104611
2.0	1.000000	1.000937	1.115229	1.001107

Table 4 Transverse displacement at the free end (v/L) for different models

λ	Reference [44]	Exact curvature [29]	General curvature [29]	Present
0.2	0.303958	0.303960	0.285390	0.303959
0.4	0.549866	0.549872	0.521884	0.549866
0.6	0.694455	0.694466	0.674109	0.694454
0.8	0.719785	0.719804	0.727215	0.719793
1.0	0.636620	0.636648	0.686816	0.636670
1.2	0.479856	0.479920	0.574715	0.480013
1.4	0.297623	0.297869	0.422559	0.297952
1.6	0.137466	0.137841	0.264570	0.137948
1.8	0.033773	0.034114	0.130552	0.034202
2.0	0.000000	0.000061	0.040505	-0.000043

which is consistent with the trends reported in the literature. Nevertheless, the present formulation maintains close agreement with the exact curvature model over the considered loading range. In contrast, the general curvature model exhibits noticeable deviations as the bending moment increases, particularly in the large deformation regime, which can be attributed to its simplified curvature expression with reduced coupling between deformation measures. Despite this, the present model continues to closely follow the exact curvature results, demonstrating its capability to accurately capture strong geometric nonlinearity.

Fig. 8 depicts the deformed configurations corresponding to different bending moments. When the moment parameter reaches $\lambda = 2$, the beam deforms into a shape that closely approximates a full circle, indicating that the proposed element is capable of capturing extreme bending deformations.

5.4 Torsion of a cantilever beam

Finally, a torsion-dominated problem is considered to examine the performance of the proposed beam element in modeling large twist deformation. A torque is applied at the free end to induce a total rotation of 180 degrees of the cross-section. The torque

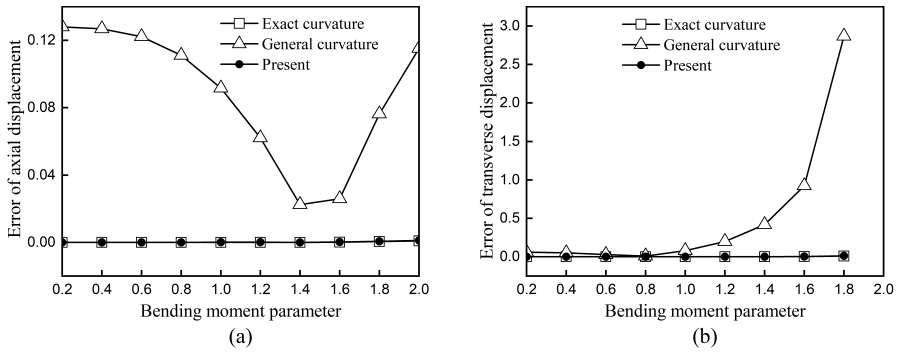


Fig. 7 Comparison of relative errors predicted by the exact curvature model, general curvature model, and the present model under different non-dimensional bending moment parameters: (a) relative error of axial displacement, (b) relative error of transverse displacement.

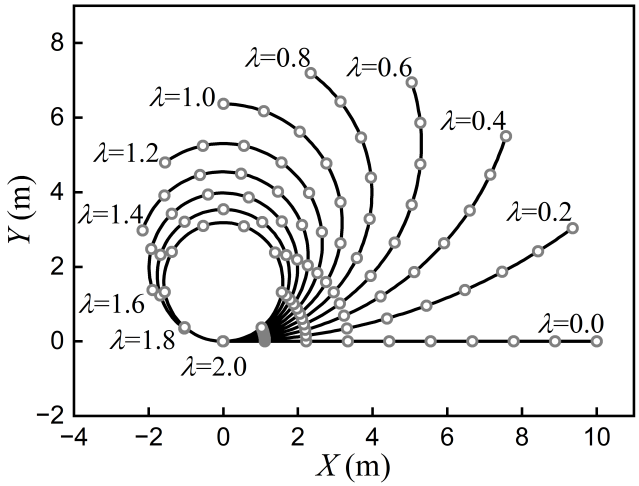


Fig. 8 Cantilever beam subjected to different bending moments at the free end.

required to produce at the free end can be expressed as

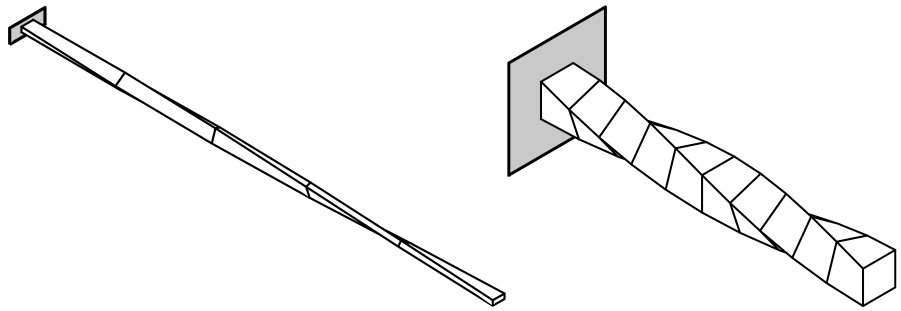
$$T = \frac{\pi G I_{\mathrm{p}}}{L}. \tag{35}$$

Two cantilever beams with different slenderness ratios are analyzed. The first beam has a length of 0.254 m, a rectangular cross-section of 0.00254 m × 0.00635 m, a slenderness ratio of 100, a Young's modulus of 6.9×10^{11} Pa, and is discretized into 5 elements. The second beam has a length of 1 m, a square cross-section of 0.1 m × 0.1 m, a slenderness ratio of 10, a Young's modulus of 8.2×10^{10} Pa, and is discretized into 10 elements. The twist angle of the beam cross-section relative to the undeformed configuration is defined based on the change in orientation of the cross-sectional normal

vectors. It is evaluated as

$$\theta = \frac{180^\circ}{\pi} \arctan\left(\frac{\mathbf{t}_0 \cdot (\mathbf{n}_0 \times \mathbf{n}_1)}{\mathbf{n}_0 \cdot \mathbf{n}_1}\right) \tag{36}$$

where $\mathbf{t}_0$ denotes the unit tangent vector of the beam centerline in the initial configuration, $\mathbf{n}_0$ and $\mathbf{n}_1$ are the unit normal vectors of the cross-section in the initial and deformed configurations, respectively.



(a) (b)

Fig. 9 Cantilever beam subjected to a 180-degree twist at the free end: (a) slenderness ratio of 100, (b) slenderness ratio of 10.

In Fig. 9, the deformed configurations of the two beams are presented, where the torsional angles are 179.2643° and 179.9705° , respectively. The results indicate that the proposed element is capable of accurately capturing large torsional deformation for beams with significantly different slenderness characteristics, without exhibiting numerical instability or loss of accuracy.

6 Conclusions

This paper proposed a gradient-deficient geometrically exact beam element formulated within the framework of the ANCF. By employing the axial gradient and a single transverse gradient to construct the cross-sectional coordinate system, the element achieves a reduced kinematic representation without introducing rotational parameters or compromising geometric exactness.

The resulting formulation preserves the essential structural characteristics required for large-rotation and large-deformation analyses. By eliminating one transverse gradient, a more compact set of generalized coordinates is achieved, while accurate representations of bending and torsional deformation are retained.

Numerical studies covering static large deflection, rolling-up behavior, and torsional response demonstrate that the gradient-deficient element delivers results in close agreement with results from existing models. These examples confirm that the proposed formulation maintains reliability across different deformation modes while benefiting from reduced model complexity.

Overall, the beam element provides an efficient and systematic alternative to conventional ANCF beam formulations, particularly for applications where torsional effects and computational efficiency are of primary concern. The formulation also offers a basis for further extensions toward reduced-coordinate ANCF elements and large-scale flexible multibody system simulations.

Statements and declarations

- Competing interests

The authors declare no competing interests.

- Data availability

All data generated or analyzed during this study are included in this published article.

References

[1] Shabana, A.A.: An overview of the ancf approach, justifications for its use, implementation issues, and future research directions. Multibody Syst. Dyn. **58**(3-4), 433–477 (2023)

[2] Otsuka, K., Makihara, K., Sugiyama, H.: Recent advances in the absolute nodal coordinate formulation: Literature review from 2012 to 2020. J. Comput. Nonlinear Dyn. **17**(8), 18 (2022)

[3] Hu, W., Deng, Z.: A review of dynamic analysis on space solar power station. Astrodynamics **7**(2), 115–130 (2023)

[4] Liu, C., Tian, Q., Yan, D., Hu, H.: Dynamic analysis of membrane systems undergoing overall motions, large deformations and wrinkles via thin shell elements of ancf. Comput. Meth. Appl. Mech. Eng. **258**(1), 81–95 (2013)

[5] Zhao, Z., Ren, G.: A quaternion-based formulation of euler–bernoulli beam without singularity. Nonlinear Dyn. **67**(3), 1825–1835 (2012)

[6] Fan, W., Zhu, W.D.: An accurate singularity-free formulation of a three-dimensional curved euler-bernoulli beam for flexible multibody dynamic analysis. J. Vib. Acoust.-Trans. ASME **138**(5), 051001 (2016)

[7] Borkovi, A., Gfrerer, M.H., Marussig, B.: Geometrically exact isogeometric bernoulli–euler beam based on the frenet–serret frame. Comput. Meth. Appl. Mech. Eng. **405**, 115848 (2023)

[8] Liu, B., Ji, Y.: Nonlinear dynamics of three-dimensional curved geometrically exact beams by a quadrature element formulation. Nonlinear Dyn. **112**(17), 14925–14958 (2024)

[9] Debeurre, M., Grolet, A., Thomas, O.: Quaternion-based finite-element computation of nonlinear modes and frequency responses of geometrically exact beam structures in three dimensions. Multibody Syst. Dyn. **63**(4), 557–594 (2025)

[10] Jeleni, G., Crisfield, M.A.: Interpolation of rotational variables in nonlinear dynamics of 3d beams. Int. J. Numer. Methods Eng. **43**(7), 1193–1222 (2015)

[11] Fan, W., Zhu, W.D., Ren, H.: A new singularity-free formulation of a three-dimensional euler–bernoulli beam using euler parameters. J. Comput. Nonlinear Dyn. **11**(4), 041013 (2016)

[12] Pai, P.F.: Problems in geometrically exact modeling of highly flexible beams. Thin-Walled Struct. **76**, 65–76 (2014)

[13] Shabana, A.A., Hussien, H.A., Escalona, J.L.: Application of the absolute nodal coordinate formulation to large rotation and large deformation problems. J. Mech. Des. **120**(2), 188–195 (1998)

[14] Gerstmayr, J., Sugiyama, H., Mikkola, A.: Review on the absolute nodal coordinate formulation for large deformation analysis of multibody systems. J. Comput. Nonlinear Dyn. **8**(3), 031016 (2013)

[15] Dombrowski, S.V.: Analysis of large flexible body deformation in multibody systems using absolute coordinates. Multibody Syst. Dyn. **8**(4), 409–432 (2002)

[16] Berzeri, M., Shabana, A.A.: Development of simple models for the elastic forces in the absolute nodal co-ordinate formulation. J. Sound Vibr. **235**(4), 539–565 (2000)

[17] Yoo, W.S., Dmitrochenko, O., Park, S.J., Lim, O.K.: A new thin spatial beam element using the absolute nodal coordinates: Application to a rotating strip. Mech. Based Des. Struct. Mech. **33**(3-4), 399–422 (2005)

[18] Wang, Y., Ma, Z., Wu, M., Shen, Z.: On the use of higher-order ancf beam elements in modeling solid rods with various cross-section configurations. Acta Mech. **237**(1), 317–334 (2025)

[19] Bocko, J., Pleško, P., Delyová, I., Sivák, P.: Comparison of structural analysis of thin-walled structures accomplished by isogeometric analysis and the finite element method. Materials **15**(19), 6516 (2022)

[20] Ebel, H., Matikainen, M.K., Hurskainen, V.V., Mikkola, A.: Higher-order beam elements based on the absolute nodal coordinate formulation for three-dimensional elasticity. Nonlinear Dyn. **88**(2), 1075–1091 (2017)

[21] Li, H., Zhong, H.: Weak form quadrature elements based on absolute nodal coordinate formulation for planar beamlike structures. Acta Mech. **232**(11), 4289–4307

(2021)

[22] Shen, Z., Li, P., Liu, C., Hu, G.: A finite element beam model including cross-section distortion in the absolute nodal coordinate formulation. Nonlinear Dyn. **77**(3), 1019–1033 (2014)

[23] Shen, Z.: Thin-walled composite beam elements via the absolute nodal coordinate formulation. Multibody Syst. Dyn. **62**(1), 107–135 (2024)

[24] Tang, Y., Tian, Q., Hu, H.: Efficient modeling and order reduction of new 3d beam elements with warping via absolute nodal coordinate formulation. Nonlinear Dyn. **109**(4), 2319–2354 (2022)

[25] Shabana, A.A., Desai, C.J., Grossi, E., Patel, M.: Generalization of the strain-split method and evaluation of the nonlinear ancf finite elements. Acta Mech. **231**(4), 1365–1376 (2020)

[26] Patel, M., Shabana, A.A.: Locking alleviation in the large displacement analysis of beam elements: the strain split method. Acta Mech. **229**(7), 2923–2946 (2018)

[27] Lan, P., Tian, Q., Yu, Z.: A new absolute nodal coordinate formulation beam element with multilayer circular cross section. Acta Mech. Sin. **36**(1), 82–96 (2020)

[28] Orzechowski, G.: Analysis of beam elements of circular cross section using the absolute nodal coordinate formulation. Arch. Mech. Eng. **59**(3), 283–296 (2012)

[29] Zhang, D., Luo, J.: A comparative study of geometrical curvature expressions for the large displacement analysis of spatial absolute nodal coordinate formulation euler–bernoulli beam motion. Proc. Inst. Mech Eng Pt K-J Multi-Body Dyn. **233**(3), 631–641 (2018)

[30] Ren, H., Yang, K.: A referenced nodal coordinate formulation. Multibody Syst. Dyn. **51**, 305–342 (2021)

[31] Gerstmayr, J., Shabana, A.A.: Analysis of thin beams and cables using the absolute nodal co-ordinate formulation. Nonlinear Dyn. **45**(1), 109–130 (2006)

[32] Zemljarič, B., Ažbe, V.: Analytically derived matrix end-form elastic-forces equations for a low-order cable element using the absolute nodal coordinate formulation. J. Sound Vibr. **446**, 263–272 (2019)

[33] Hara, K., Watanabe, M.: Development of an efficient calculation procedure for elastic forces in the ancf beam element by using a constrained formulation. Multibody Syst. Dyn. **43**(4), 369–386 (2018)

[34] Chen, Y., Zhang, D., Li, L.: Dynamic analysis of rotating curved beams by using absolute nodal coordinate formulation based on radial point interpolation

method. J. Sound Vibr. **441**, 63–83 (2019)

[35] Sheng, F., Zhong, Z., Wang, K.H.: Theory and model implementation for analyzing line structures subject to dynamic motions of large deformation and elongation using the absolute nodal coordinate formulation (ancf) approach. Nonlinear Dyn. **101**(1), 333–359 (2020)

[36] Sugiyama, H., Gerstmayr, J., Shabana, A.A.: Deformation modes in the finite element absolute nodal coordinate formulation. J. Sound Vibr. **298**(4), 1129–1149 (2006)

[37] Gerstmayr, J., Irschik, H.: On the correct representation of bending and axial deformation in the absolute nodal coordinate formulation with an elastic line approach. J. Sound Vibr. **318**(3), 461–487 (2008)

[38] Sugiyama, H., Koyama, H., Yamashita, H.: Gradient deficient curved beam element using the absolute nodal coordinate formulation. J. Comput. Nonlinear Dyn. **5**(2), 1090–1097 (2010)

[39] Liu, C., Tian, Q., Hu, H.: New spatial curved beam and cylindrical shell elements of gradient-deficient absolute nodal coordinate formulation. Nonlinear Dyn. **70**(3), 1903–1918 (2012)

[40] Dufva, K.E., Sopanen, J.T., Mikkola, A.M.: Three-dimensional beam element based on a cross-sectional coordinate system approach. Nonlinear Dyn. **43**(4), 311–327 (2006)

[41] Gruber, P.G., Nachbagauer, K., Vetyukov, Y., Gerstmayr, J.: A novel director-based bernoulli–euler beam finite element in absolute nodal coordinate formulation free of geometric singularities. Mech. Sci. **4**(2), 279–289 (2013)

[42] Ebrahimi, M., Butscher, A., Cheong, H.: A low order, torsion deformable spatial beam element based on the absolute nodal coordinate formulation and bishop frame. Multibody Syst. Dyn. **51**, 247–278 (2021)

[43] Otsuka, K., Wang, Y., Fujita, K., Nagai, H., Makihara, K.: Multifidelity modeling of deployable wings: Multibody dynamic simulation and wind tunnel experiment. AIAA J. **57**(10), 4300–4311 (2019)

[44] Mattiasson, K.: Numerical results from large deflection beam and frame problems analysed by means of elliptic integrals. Int. J. Numer. Methods Eng. **17**(1), 145–153 (2010)

[45] Sonneville, V., Brüls, O.: A few good reasons to consider a beam finite element formulation on the lie group se(3). (2013). Paper presented at the ASME 2013 International Design Engineering Technical Conferences and Computers and Information in Engineering Conference, Portland, Oregon, USA, 4-7 August 2013.